ATLAS NOTE

ATLAS-CONF-2011-015

March 9, 2011

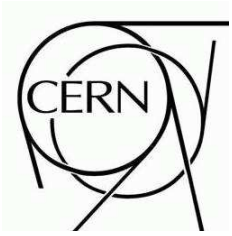

Measurement of the W^+W^- production cross section in proton-proton collisions at $\sqrt{s} = 7$ TeV with the ATLAS detector

The ATLAS Collaboration

Abstract

We report a measurement of the W^+W^- production cross section in pp collisions at $\sqrt{s}$ =7 TeV. The W^+W^- leptonic decay channels are analyzed using data corresponding to 35 pb^{-1} of integrated luminosity collected by the ATLAS detector during 2010 at the CERN Large Hadron Collider. With eight observed W^+W^- candidate events and an estimated background of 1.7$\pm$0.6 events, the measured W^+W^- production cross section is 40^{+20}_{-16}(stat)$\pm$7(syst) pb. The probability for the estimated background to fluctuate up to at least the observed number of events is 1.4×10^{-3}, corresponding to a signal significance of 3.0 standard deviations.

1 Introduction

The measurement of the W^+W^- production cross section at the LHC provides an important test of the Standard Model (SM) through the sensitivity to the triple gauge boson couplings that result from the non-Abelian structure of the gauge symmetry group, $SU(2)_{\rm L} \times U(1)_{\rm Y}$. Furthermore, non-resonant W^+W^- production is an irreducible background in searches for the Higgs boson in the same final state. Understanding the detection sensitivity of ATLAS to W-pair production is crucial for Higgs boson searches.

The leading-order Feynman diagrams for the dominant $q\bar{q}' \to W^+W^-$ production mechanisms at the LHC are shown in the left and middle diagrams of Fig. 1. The corresponding next-to-leading order (NLO) prediction of the total cross section $\sigma(q\bar{q}',\ q\bar{q} \to W^+W^-)$ is 44.9±2.2 pb at $\sqrt{s}$ = 7 TeV [1–6]. Gluon-gluon fusion through quark loops, shown in the right diagram, contributes an additional 3% of the event rate to the total non-resonant W^+W^- production.

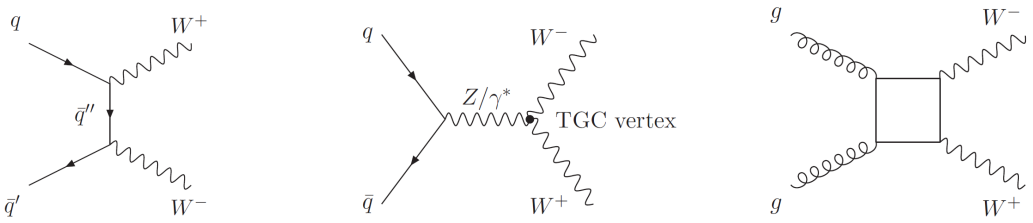

Figure 1: The SM tree-level Feynman diagrams for W^+W^- production through the $q\bar{q}$ initial state (the left and middle diagrams). The s-channel diagram, in the middle, contains the WWZ and $WW\gamma$ triple gauge boson coupling (TGC) vertices. The gluon-gluon fusion process, mediated by quark loops, is shown in the right diagram.

We reconstruct the W^+W^- events using leptonic decays of the W boson: $W^\pm \to \ell^\pm\nu$, where ℓ is an electron or muon. Sequential decays to electrons and muons via τ leptons are also included as signal: $W^\pm \to \tau^\pm\nu_\tau \to \ell^\pm\nu_\ell\nu_\tau$. The resulting final state has two high-transverse-momentum (high-$p_{\rm T}$) charged leptons and substantial transverse momentum imbalance in the final state (referred to as missing transverse energy $E_{\rm T}^{\rm miss}$ below) due to the neutrinos or antineutrinos escaping detection.

The major backgrounds for this $\ell^+\ell^-E_{\rm T}^{\rm miss}$ final state are Drell-Yan, top quark, W+jet and diboson (WZ, ZZ and $W\gamma$) production. A set of event selection criteria is designed and optimized to achieve good W^+W^- signal detection sensitivity. A brief description is given below – more detailed information can be found in later sections.

- **Drell-Yan**
  Resonant (Z boson) and non-resonant Drell-Yan processes yield charged-lepton pairs with associated hadronic jets. This background has two high-$p_{\rm T}$ charged leptons and false missing transverse energy, either from the mismeasurement of the charged leptons, mismeasurement of the associated hadronic activity, or both. There is also a contribution from $Z \to \tau^+\tau^-$. We reduce this background by removing lepton pairs consistent with Z boson decays, vetoing events with high-$p_{\rm T}$ jet activity, and imposing a stringent requirement on the missing transverse energy.

- **Top**
  W^+W^- pairs are produced in association with additional jets in top quark production processes such as $t\bar{t}$ or W^-t and $W^+\bar{t}$. This is considered to be a background in this analysis. It is suppressed in the event selection by vetoing on high-$p_{\rm T}$ jets; the W^+W^- signal cross section is therefore extrapolated to include higher jet multiplicities.

- **W+ jets**
  $W+$ jets denotes the production of a W boson with associated hadronic jets. The leptonic decay of the W produces a high-p_{T} charged lepton and missing transverse energy; a second "fake" charged lepton can come from a jet misidentified as a lepton. Stringent charged lepton selection criteria are used to reduce this misidentification background.

- **Diboson**
  The diboson background comprises $W^{\pm}Z$, ZZ and $W^{\pm}\gamma$. In this case there can be high-p_{T} charged leptons and missing transverse energy *e.g.,* $W^{\pm} \to e^{\pm}\nu_e$ with $Z \to e^{+}e^{-}$, or there can be a high-p_{T} charged lepton and missing transverse energy and a photon misidentified as an electron. These backgrounds are reduced by the criteria listed above and by accepting events with exactly two high-p_{T} leptons.

The signal acceptance and efficiencies are determined using Monte Carlo (MC) simulations. Detailed comparisons of MC predicted efficiencies to the efficiencies measured from data control samples such as $Z \to \ell^{+}\ell^{-}$ are used to determine scale factors. These scale factors are then used to correct the MC predictions of efficiencies and acceptances for both signal and background events.

The background contributions to the final signal sample are determined with a combination of high-statistics MC samples and estimates determined directly from data. The $W^{+}W^{-}$ production cross section is then extracted from the observed number of events, the estimated background, the $W^{+}W^{-}$ signal detection acceptance and efficiency, and the integrated luminosity.

2 The ATLAS detector and data sample

The ATLAS detector [7] is a multipurpose particle physics apparatus with nearly 4π solid angle coverage. ATLAS uses a right-handed coordinate system with its origin at the nominal interaction point (IP) in the centre of the detector and the z-axis along the beam pipe. The x-axis points from the IP to the centre of the LHC ring, and the y axis points upward. Cylindrical coordinates (r,ϕ) are used in the transverse plane, ϕ being the azimuthal angle around the beam pipe. The pseudorapidity is defined in terms of the polar angle θ as $\eta = -\ln[\tan(\theta/2)]$. Closest to the beamline are inner tracking detectors (ID) which use layers of silicon-based and straw-tube detectors, located inside a thin superconducting solenoid that provides a 2T magnetic field, to measure the trajectories of charged particles within $|\eta| < 2.5$. The solenoid is surrounded by a hermetic calorimeter system. A liquid argon (LAr) sampling calorimeter is divided into a central barrel calorimeter and two end-cap calorimeters, each housed in a separate cryostat. Fine-grained LAr electromagnetic (EM) calorimeters, with excellent energy resolution, provide coverage for $|\eta|$ <3.2. An iron-scintillator tile calorimeter provides hadronic coverage in the range $|\eta|$ <1.7. In the end-caps ($|\eta|$ >1.5), LAr hadronic calorimeters match the outer $|\eta|$ limits of the end-cap EM calorimeters. LAr forward calorimeters provide both EM and hadronic energy measurements, and extend the coverage to $|\eta|$ <4.9. Outside the calorimeters is an extensive muon spectrometer (MS) in a toroidal magnetic field within $|\eta| < 2.7$. The muon trigger system covers the range $|\eta|$ <2.4.

A three-level trigger system is used to select interesting events in real time. The Level-1 trigger is implemented in hardware and uses a subset of detector information to reduce the event rate to a design value of at most 75 kHz. This is followed by two software-based trigger levels, Level-2 and the Event Filter, which together reduce the event rate to about 200 Hz.

Only data where all subsystems described above are fully operational are used. Applying these requirements to $\sqrt{s} = 7$ TeV pp collision data taken in stable beam conditions and recorded during 2010 results in a data sample of 35 pb^{-1}. This luminosity value has a relative uncertainty of 11% [8].

3 Online sample selection

The trigger system selects events online by requiring either an electron that deposits at least 15 GeV of transverse energy in the calorimeter or a muon that is detected with a transverse momentum of at least 13 GeV. Using these single lepton triggers, the resulting trigger efficiencies for the ee, $\mu\mu$ and $e\mu$ final states are close to 100% for leptons with p_{T} greater than 20 GeV. These efficiencies are determined using data control samples of $Z \to \ell^+\ell^-$ events. The trigger efficiencies in MC are scaled by the ratio of the measured trigger efficiency in data to that in simulation. The resulting ratios (called MC scale factors) for the three di-lepton channels are consistent with unity and have a negligible combined statistical and systematic uncertainty.

4 Simulated data samples

Monte Carlo simulation samples are used to develop and validate the analysis procedures, to calculate the acceptance for W^+W^- events and to evaluate the contributions from some background processes.

For the W^+W^- signal, we use the next-to-leading order (NLO) generator MC@NLO [9] in conjunction with the CTEQ6.6 [10] parton distribution functions (PDF). HERWIG [11] is used for W leptonic decays and for the parton shower simulation and hadronization. Jimmy [12] is used for the underlying event simulation. In addition, the `gg2ww` [13] MC generator (interfaced to HERWIG and Jimmy) is used to simulate the W^+W^- events from the gluon-gluon fusion process.

The Drell-Yan and the $W+$ jets backgrounds are generated with ALPGEN, which implements the exact leading-order matrix elements for final states with up to six partons. Additional simulation samples produced with the PYTHIA and MC@NLO generators are used to cross check the Drell-Yan background contributions. The top ($t\bar{t}$ and Wt) and diboson (WZ and ZZ) backgrounds are modeled with MC@NLO interfaced to the HERWIG and Jimmy programs. The $W\gamma$ and hadronic multi-jet backgrounds are modeled with the PYTHIA generator.

The detector response for all the generated MC events is simulated by passing them through a detailed simulation [14] of the ATLAS detector based on the `GEANT4` program [15]. These simulated data samples are then reconstructed, selected, and analyzed as done for the data.

In this analysis, the MC event samples are normalized to an integrated luminosity of 35 pb^{-1} using SM NLO cross sections. The total cross section of W^+W^- production is normalized to 46 pb for signal predictions, which includes the production processes from the $q\bar{q}'$ and the gg initial states.

5 Object reconstruction

Brief descriptions of the relevant physics objects used in this analysis are given in this section. These objects are the pp collision vertices, electrons, muons, missing transverse energy, and hadronic jets.

5.1 pp collision vertices

The pp collision vertices in each bunch crossing are reconstructed using the inner tracking system. If multiple collision vertices are reconstructed, we select the vertex with the largest sum p_{T}^2 of the associated tracks as the primary vertex. To remove cosmic-ray and beam-induced backgrounds, we require the primary vertex to have at least three tracks. This requirement reduces the signal acceptance by about 0.1%.

5.2 Electrons

Electron candidates are formed by matching a cluster of energy in the electromagnetic calorimeter to a charged track found in the inner tracking system. In this analysis, we use electrons with $|\eta| < 1.37$ or $1.52 < |\eta| < 2.47$, which avoids the transition region between the barrel and the end-cap electromagnetic calorimeters.

We use the ATLAS "tight" electron identification criteria [16]. These criteria are based on calorimeter shower shape, inner-detector track quality, detection of transition radiation, track-to-calorimeter-cluster matching, and the ratio E/p, where E is the calorimeter cluster energy and p is the track momentum.

In this analysis, the electron E_{T} is required to exceed 20 GeV, where the E_{T} measurement is based on the calorimeter energy and the associated track direction. To further reduce backgrounds due to hadrons mimicking the electron signature, we impose an isolation requirement on the electron. The isolation requirement is that the sum of calorimeter cells' energy within a cone $\Delta R = \sqrt{(\Delta\eta)^2 + (\Delta\phi)^2}$ of 0.3 around the electron, excluding the energy in the electron cluster, must be less than 6 GeV. In addition, the longitudinal impact parameter $|z_0|$ of the track relative to the primary vertex must be smaller than 10 mm, and the transverse impact parameter significance d_0/σ_{d_0} must be less than 10, where d_0 and σ_{d_0} are the transverse impact parameter relative to the primary vertex and its uncertainty, respectively.

The electron identification efficiency is measured in data using control samples of $Z \to e^+e^-$ and $W^\pm \to e^\pm\nu$ events. The overall electron selection efficiency in this analysis is about 78% for the central region ($|\eta| < 0.8$), and decreases to about 64% in the forward region ($2.0 < |\eta| < 2.47$). The statistical uncertainty for these measurements is less than 0.4%. The corresponding systematic uncertainty is about 5% which is dominated by the variations of electron detection efficiencies as a function of η and E_{T}.

5.3 Muons

Muons are reconstructed using information from the muon spectrometer, the inner tracking detectors, and the calorimeters. Muon candidates are formed using an algorithm that associates the MS track with the corresponding ID track, after the former is corrected for the energy loss in the calorimeter. The absolute value of the pseudorapidity $|\eta|$ of the combined muon is required to be less than 2.4. To reject muons from charged π or K decays and charged particles from the beam-induced backgrounds, the muon transverse momentum measured in the MS must exceed 10 GeV and be consistent with the ID measurement ($|p_{\mathrm{T}}^{\mathrm{ID}} - p_{\mathrm{T}}^{\mathrm{MS}}|/p_{\mathrm{T}}^{\mathrm{ID}} < 0.5$). The muon transverse momentum of the combined MS and ID systems must be greater than 20 GeV. To suppress muons originating from hadronic jets, the muons must be isolated such that the p_{T} sum of other tracks in a cone of $\Delta R = 0.2$ around the muon track scaled by the muon p_{T} is less than 0.1.

The muon reconstruction and identification efficiencies are measured using $Z \to \mu^+\mu^-$ candidates in data. The efficiencies are determined for the MS muon reconstruction, ID muon reconstruction and muon isolation. The overall muon reconstruction efficiency is found to be 92%$\pm$0.4%(stat)$\pm$1.0%(syst) in data. The statistical uncertainty is due to the statistics of the Z sample in the data, and the systematic uncertainty is dominated by the efficiency variations in different run periods.

5.4 Hadronic jets

Jets are reconstructed from calorimeter clusters using the anti-k_t algorithm [17–19] with a jet resolution parameter of $\Delta R = 0.4$. These jets are calibrated using p_{T}- and η-dependent correction factors [20] based on MC simulation, and validated by extensive test beam and collision data. The selected jets are required to have $p_{\mathrm{T}} > 20$ GeV and $|\eta| < 3$. The jet energy scale uncertainty depends on p_{T} and η and is less than 10% for $p_{\mathrm{T}} > 20$ GeV and $|\eta| < 2.8$ [20].

5.5 Missing transverse energy

The missing transverse energy is reconstructed using calorimeter energies from clusters in the detection range $|\eta| < 4.5$ and muon momenta measured by the muon spectrometer and inner detector. The mis-measured energies of leptons or jets can produce false $E_{\mathrm{T}}^{\mathrm{miss}}$. To reduce the rate of backgrounds that arise from these mis-measurements—particularly the Drell-Yan background—we use a relative missing transverse energy ($E_{\mathrm{T,\,Rel}}^{\mathrm{miss}}$), which is defined as as follows:

$$E_{\mathrm{T,\,Rel}}^{\mathrm{miss}} = \begin{cases} E_{\mathrm{T}}^{\mathrm{miss}} \times \sin\left(\Delta\phi_{\ell,j}\right) & \text{if } \Delta\phi < \pi/2 \\ E_{\mathrm{T}}^{\mathrm{miss}} & \text{if } \Delta\phi \geq \pi/2, \end{cases} \tag{1}$$

where $\Delta\phi_{\ell,j}$ is the difference in the azimuthal angle ϕ between the $E_{\mathrm{T}}^{\mathrm{miss}}$ and the nearest lepton or jet. This requirement also reduces the background from $Z \rightarrow \tau^{+}\tau^{-}$, where the real $E_{\mathrm{T}}^{\mathrm{miss}}$ from the τ semileptonic decays is parallel to the momenta of the leptons.

6 Event selection

Di-lepton events are selected using the lepton identification requirements described in the previous section. For each di-lepton final state (ee, or $\mu\mu$, or $e\mu$), we require each electron (or muon) to have E_{T} (or p_{T}) > 20 GeV, and we require exactly two leptons with opposite charges. Both leptons are required to originate from the primary vertex. The leptons must also have a minimum separation (effectively imposed by the lepton isolation requirement) in $\eta - \phi$ space of $\Delta R > 0.3$ in the ee channel and $\Delta R > 0.2$ in the $\mu\mu$ and the $e\mu$ channels.

Figure 2 shows the comparisons of the invariant mass distributions between data and MC for the ee candidates (left plot) and the $\mu\mu$ candidates (right plot).

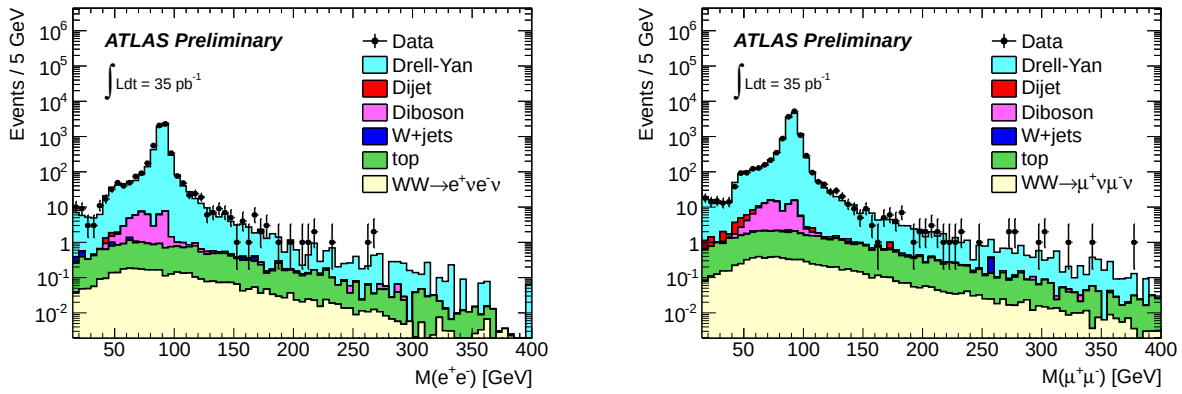

Figure 2: The invariant mass distributions for ee (left) and $\mu\mu$ (right) di-lepton final states. The points represent data and the stacked histograms are the MC predictions, which are normalized to 35 pb^{-1} using SM cross sections.

As observed in Fig. 2, after the di-lepton selection, the dominant contribution (>97%) to ee and $\mu\mu$ events comes from the inclusive $Z \rightarrow \ell^{+}\ell^{-}$ process. To reduce this background and the background from hadronic multi-jets, the invariant mass of the dilepton pair ($e^{+}e^{-}$ or $\mu^{+}\mu^{-}$) is required to exceed 15 GeV and is not allowed to be within $\pm$10 GeV of the Z-mass.

As shown in Fig. 3, further suppression of the remaining Drell-Yan and other backgrounds is achieved by requiring $E_{\mathrm{T,\,Rel}}^{\mathrm{miss}}$ >40 GeV for the ee and $\mu\mu$ channels and $E_{\mathrm{T,\,Rel}}^{\mathrm{miss}} > 20$ GeV for the $e\mu$ channel. The

top row of this figure shows the $E_{\mathrm{T,\,Rel}}^{\mathrm{miss}}$ distribution prior to applying the jet-veto selection criteria (defined below) for the ee and $\mu\mu$ channels combined (left) and the $e\mu$ (right) channel.

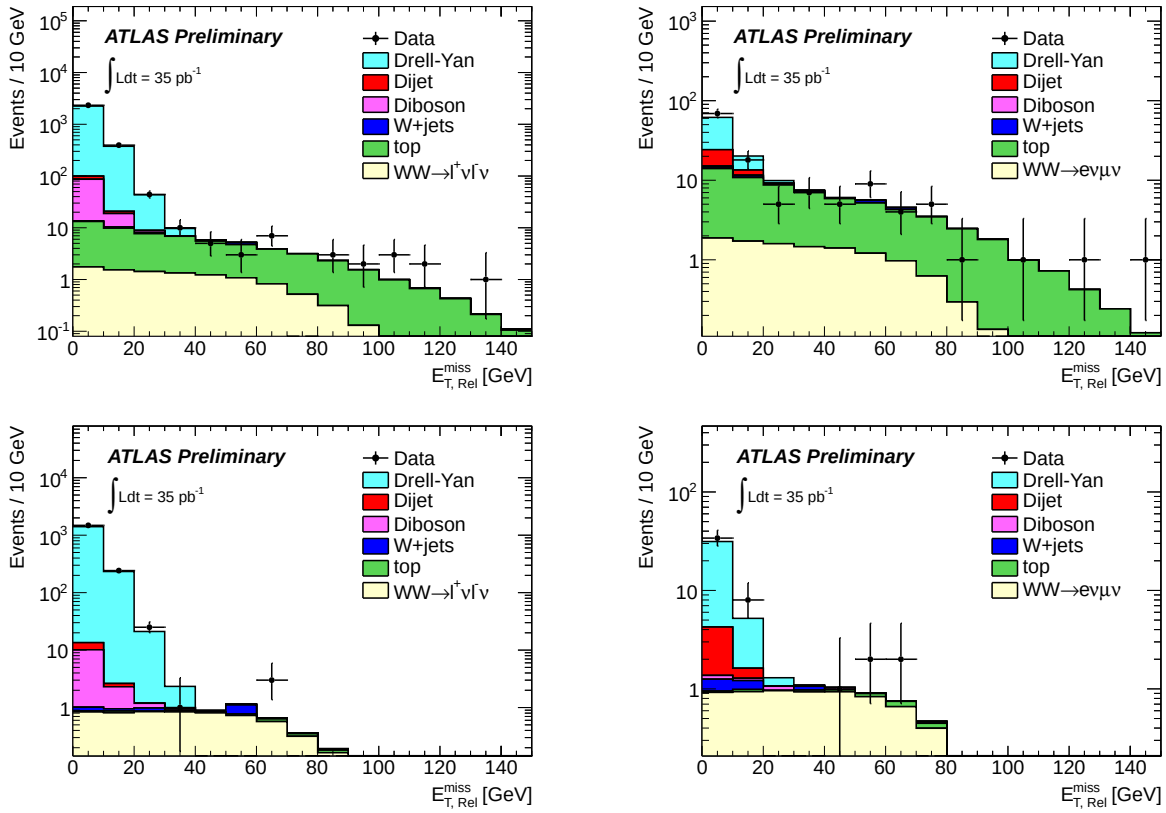

Figure 3: $E_{\mathrm{T,\,Rel}}^{\mathrm{miss}}$ distributions for the selected ee and $\mu\mu$ (left) and $e\mu$ (right) samples after the Z mass veto cut (top row). The bottom row shows the same distributions for events containing no hadronic jets with $p_{\mathrm{T}} > 20$ GeV and $|\eta| < 3$.

Suppression of the top background is accomplished by rejecting events containing jets with $p_{\mathrm{T}} > 20$ GeV and $|\eta| < 3$ (the jet-veto requirement). The bottom row of Fig. 3 shows the $E_{\mathrm{T,\,Rel}}^{\mathrm{miss}}$ distributions for events after applying the jet-veto requirement. Figure 4 shows that the majority of the W^+W^- signal is in the zero-jet bin of the jet multiplicity distribution, while the top events populate the higher jet multiplicity bins.

Table 1 shows the numbers of candidates remaining after the various W^+W^- event selection criteria are applied. After all the selection criteria are applied to the di-lepton samples, eight W^+W^- candidate events remain: one in the ee channel, two in the $\mu\mu$ channel, and five in the $e\mu$ channel.

7 Signal acceptance

The signal acceptance is one of the key ingredients for determining the W^+W^- cross section. Determining this acceptance relies on detailed MC signal modeling and event selection efficiency corrections using control data samples, as described in previous sections. These corrections differ by at most a few percent from unity, indicating the inherent accuracy of the simulation. Detailed information on the W^+W^- event selection acceptance is provided below.

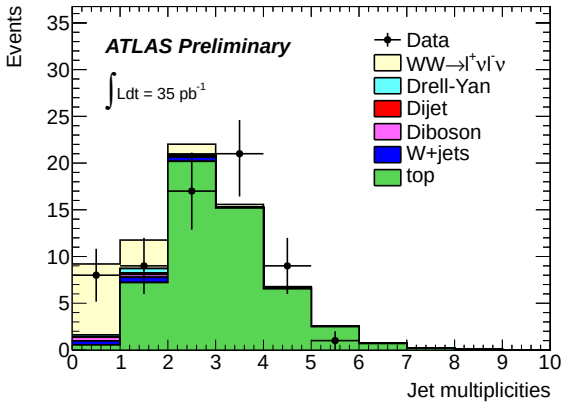

Figure 4: Jet multiplicity distribution for events passing the full W^+W^- selection before the application of the jet-veto requirement. Here jets must have $p_{\mathrm{T}} > 20$ GeV and $|\eta| < 3$. The points represent the data and the stacked histograms are the MC predictions.

Cuts	e^+e^-+$E_{\mathrm{T}}^{\mathrm{miss}}$	$\mu^+\mu^-$ +$E_{\mathrm{T}}^{\mathrm{miss}}$	$e^\pm\mu^\mp$ +$E_{\mathrm{T}}^{\mathrm{miss}}$
2 leptons (SS and OS)	6096	12802	134
2 leptons (OS)	6057	12798	126
$M_{\ell\ell} > 15$ GeV	6044	12724	-
Z veto ($\lvert M_{\ell\ell} - M_Z\rvert > 10$ GeV)	872	1935	-
$E_{\mathrm{T,\,Rel}}^{\mathrm{miss}}$ cut	12	14	39
Jet veto (No. of jet=0)	1	2	5

Table 1: The number of candidates remaining in the data after applying the W^+W^- selection criteria in the three di-lepton channels. The notation SS and OS denotes candidates with same-sign and opposite-sign charges.

Table 2 shows the number of MC W^+W^- events passing each selection cut for the three di-lepton channels. The MC events shown in the table are normalized to 35 pb^{-1} using the SM W^+W^- production cross sections with $q\bar{q}'$ and gg initial states.

In addition to corrections for lepton identification efficiencies in MC, we also apply a MC acceptance correction to account for the difference in the jet-veto efficiency between data and MC. Signal events may fail the jet-veto requirement if initial-state radiation (ISR) from the incoming partons produces a jet that satisfies the jet-veto requirements. The simulation may not predict this rate accurately, either because the rate of ISR is not quite correct, or because the jet-energy scale in data and in the simulation are not the same. In order to minimize the systematic uncertainty due to these two effects, we use control samples of $Z \to \ell^+\ell^-$ data and MC to determine the jet-veto efficiency correction factor to the W^+W^- selection [21]: $\varepsilon_{WW}^{\mathrm{data}} = \varepsilon_{WW}^{\mathrm{MC}} \times f_Z$, with $f_Z = \varepsilon_Z^{\mathrm{data}}/\varepsilon_Z^{\mathrm{MC}} = 0.97 \pm 0.06$. The two efficiency numbers, $\varepsilon_Z^{\mathrm{data}}$ and $\varepsilon_Z^{\mathrm{MC}}$, are the fraction of the Z events with zero jets found in data and MC, respectively.

The overall event selection acceptances for signal events are 4.1% for $e\nu e\nu$, 8.6% for $\mu\nu\mu\nu$, and 11.5% for $e\nu\mu\nu$. The contributions from $W^+W^- \to \tau^\pm\nu\ell^\mp\nu \to \ell'^\pm\ell^\mp + n\nu$ are less than 10% of the final selected W^+W^- signal events in all three di-lepton channels.

The overall systematic uncertainty in the W^+W^- selection acceptance is 7.4% for the combination of the three di-lepton channels. This overall uncertainty includes the uncertainties due to lepton identification (4.2%), the jet-veto (6.0%), the effect of multiple interactions (0.5%) and the uncertainties of the

PDFs (including the error matrices of the CTEQ6.6 PDF sets and the differences between the CTEQ6.6 and the MSTW PDF sets) used in MC modeling (1.2%).

Cuts	$ee E_{\mathrm{T}}^{\mathrm{miss}}$ Channel		$\mu\mu E_{\mathrm{T}}^{\mathrm{miss}}$ Channel		$e\mu E_{\mathrm{T}}^{\mathrm{miss}}$ Channel	
	$e\nu e\nu$	$\tau\tau/e\tau\nu\nu$	$\mu\nu\mu\nu$	$\tau\tau/\mu\tau\nu\nu$	$e\nu\mu\nu$	$\tau\tau/\mu\tau/e\tau\nu\nu$
Total Events	18.99	7.27	18.99	7.27	37.98	14.55
2 leptons (opposite charge)	3.46	0.41	7.70	0.85	10.36	1.16
$M_{\ell\ell} > 15$ GeV & Z veto	2.93	0.34	6.43	0.69	10.36	1.16
$E_{\mathrm{T,\,Rel}}^{\mathrm{miss}}$ cut	1.21	0.11	2.76	0.21	7.17	0.74
Jet veto	0.78	0.07	1.63	0.12	4.38	0.43
Overall acceptance	4.1%	0.9%	8.6%	1.6%	11.5%	2.9%

Table 2: The number of events predicted by the MC for the W^+W^- signal ($q\bar{q}'$, $q\bar{q} \rightarrow W^+W^-$ and $gg \rightarrow W^+W^-$) for the three di-lepton channels after applying the various selection criteria. We list separately the cases when both leptons are from prompt W decay, and when one or both leptons are from cascade decays involving τs. The numbers of events are normalized to 35 pb^{-1} using the SM W^+W^- production cross sections. The overall acceptances for the different cases are given in the last row.

8 Background estimation

As described in the Introduction, the main backgrounds for the W^+W^- signal come from Drell-Yan events, top ($t\bar{t}$ and single top) production, W+jets, and diboson (WZ, ZZ, $W\gamma$ and $Z\gamma$) production. The contributions of these various backgrounds to the final W^+W^- sample are described in this section.

8.1 Drell-Yan

Drell-Yan events ($Z/\gamma^* \rightarrow \ell^+\ell^-$), like W^+W^- events, produce two high p_{T} leptons. Much of this background is removed by the di-lepton invariant mass cuts and $E_{\mathrm{T,\,Rel}}^{\mathrm{miss}}$ cuts described in Sect. 6. Given the relatively large cross section of the Drell-Yan process, it contributes a non-negligible background to the W^+W^- signal due to energy/momentum mis-measurements of the two leptons or as a result of hadronic activity in the rest of the event.

The Drell-Yan backgrounds are determined from MC events generated with ALPGEN and passed through the ATLAS detector simulation. The results are cross checked with additional MC events produced by the PYTHIA and MC@NLO generators. The systematic uncertainties are determined using a data-driven method which compares the $E_{\mathrm{T,\,Rel}}^{\mathrm{miss}}$ distributions in data and MC within the Z peak region. The distributions are found to be consistent within statistical uncertainties. As a conservative estimate of the systematic, the observed difference is combined linearly with the statistical uncertainty. This systematic uncertainty is applied to the background predictions from MC. With the assumptions that the mechanism that causes a discrepancy between data and MC is independent of the invariant mass of the two leptons, and that any discrepancy between data and MC is caused by a mis-modeling of the Drell-Yan sample, a systematic uncertainty of 64% for the Drell-Yan background estimation from the MC simulation is determined. The estimated Drell-Yan backgrounds together with statistical and systematic uncertainties are shown in Table 3.

Generator	e^+e^-	$\mu^+\mu^-$	$e^\pm\mu^\mp$	combined
ALPGEN	0.00±0.10±0.07	0.01±0.10±0.07	0.23±0.06±0.15	0.24±0.15±0.17

Table 3: MC estimated Drell-Yan contribution in the signal region of the ee, $\mu\mu$, and $e\mu$ channels. The given uncertainties are statistical (first) and systematic (second). The reported systematic uncertainties are derived from the study of data control regions.

8.2 Top

After removing the largest background from $Z/\gamma^* \to \ell^+\ell^-$ events in di-lepton samples, the dominant background is from $t\bar{t}$ and Wt production, followed by the leptonic decays of the two real W bosons in these processes. This background can be effectively suppressed by requiring that there are no jets (with $p_{\mathrm{T}} > 20$ GeV and $|\eta| < 3$). However, some top events containing only jets with p_{T} less than 20 GeV can still mimic the SM W^+W^- events.

The top backgrounds in the final W^+W^- selection are estimated using MC simulations. The estimated top contributions in the W^+W^- signal region (no hadronic jets in an event) based on the MC simulation are cross checked with two data-driven methods. In the first method, the top background in the zero jet bin is estimated using the number of observed events in the N-jet bins (where N can be 2,3 or more than 3 jets) in data and the ratio of zero-jet events over number of N-jet events in MC, $N_{\mathrm{top}}^{\mathrm{zero-jet}}(\mathrm{estimate}) = N_{\mathrm{data}}^{N-\mathrm{jet}} \times (N_{\mathrm{MC\ top}}^{\mathrm{zero-jet}}/N_{\mathrm{MC\ top}}^{N-\mathrm{jet}})$. In this method the uncertainties on luminosity and on the top cross sections cancel out in the MC ratio. The second method uses a top control sample selected using b-tagging to estimate the top contribution. All three methods give consistent top background yields. The final top background estimation and systematic uncertainties are obtained from the MC studies since these yield the overall smallest background uncertainty (statistical and systematic).

The MC estimated top background is $0.55 \pm 0.12(\mathrm{stat}) \pm 0.30(\mathrm{syst})$. The systematic uncertainty includes the uncertainties for luminosity (11%), top cross sections (12%), jet-veto efficiency due to jet-energy scale (40%), QCD ISR/FSR modeling (32%) and lepton efficiency (4.2%).

8.3 W+ jets

W bosons produced in association with a hadronic jet give rise to W^+W^- backgrounds when the jet is misidentified as a lepton. The rate at which hadronic jets are misidentified as leptons may not be accurately described in the MC. The $W+$ jets background is therefore determined from data.

The $W+$ jet background is estimated by defining a control region, similar to the W^+W^- signal selection, that is enriched in W+jet events. The $W+$ jet control region is defined using an alternative lepton definition that is rich in hadronic jets. Jet-rich electrons are defined as isolated electromagnetic clusters matched to a tracks in the inner detector that fail the electron selection described in Section 5. Jet-rich muons are defined as "combined" muons that pass a looser isolation requirement and fail the muon selection described in Section 5. Events containing one fully identified lepton and a jet passing this jet-rich lepton definition are selected. These events are then required to pass the full W^+W^- event selection, where the jet is treated as if it were a fully identified lepton. The $W+$ jets background is estimated by scaling the control sample ($N_{W+\mathrm{jet}}$) by a measured fake factor. The fake factor (f) is defined as the ratio of the rate at which jets satisfy the full lepton identification to the rate at which they satisfy the jet-enriched lepton selection. It is measured in a di-jet data sample as a function of lepton p_{T} and is found to be 0.03 (0.30) for electrons (muons) in the 20-30 GeV region. The $W+$ jets background is determined as $N_{W+\mathrm{jet}} \times f$.

Samples with same sign di-leptons are also enhanced in $W+$ jets events and are used as a control sample, with looser lepton identification, to cross check the method described above.

The $W+$ jets background estimation in the W^+W^- signal region is given in Table 4 for the three di-lepton channels. The statistical uncertainty is due to the limited statistics in the $W+$ jet control regions. In the $\mu\mu$-channel zero events are seen in the $W+$ jets control region, so the statistical uncertainty has been calculated assuming one event. The systematic uncertainty is due to the uncertainty on the determination of f. The uncertainty on f is about 36% for both electrons and muons, and is determined by the measured variations of f in different run periods and in data samples containing jets of different energies. The assigned systematic uncertainty covers variation of the quark/gluon composition of the jets in the jet data sample compared to jets in the $W+$ jets sample, and the effects of changing instantaneous luminosity on f.

The total $W+$ jets contribution to the final selected WW candidate events is estimated to be $0.54 \pm 0.32(\text{stat}) \pm 0.21(\text{syst})$.

Channel	Estimated $W+$jets background from Data
ee-channel	$0.08 \pm 0.05(\text{stat}) \pm 0.03(\text{syst})$
$\mu\mu$-channel	$0.00 \pm 0.29(\text{stat}) \pm 0.10(\text{syst})$
$e\mu$-channel	$0.46 \pm 0.12(\text{stat}) \pm 0.17(\text{syst})$
$ee + \mu\mu + e\mu$-channel	$0.54 \pm 0.32(\text{stat}) \pm 0.21(\text{syst})$

Table 4: Estimated $W+$ jets background in the W^+W^- signal region. The systematic uncertainty for the ee and $e\mu$ channels are linearly summed, based on the consideration that electron the fake factors used in ee and $e\mu$ estimations are correlated. Then, the total systematic uncertainty is the quadratic sum of (ee + $e\mu$) and $\mu\mu$.

8.4 Other background contributions

Other backgrounds to W^+W^- originate from the diboson processes WZ, ZZ and $W/Z+\gamma$. The leptonic decays of WZ and ZZ events can mimic the W^+W^- signal when one or more of the charged leptons is not reconstructed and instead contributes to $E_{\mathrm{T}}^{\mathrm{miss}}$. The $ZZ \to \ell\ell\nu\nu$ process is suppressed by the Z veto cut. The $W\gamma$ process is a background only for the ee and $e\mu$ channels, since the probability for a photon to be misidentified as a muon is negligible.

These diboson background contributions are estimated using MC simulations (MC@NLO for WZ, PYTHIA for ZZ and HERWIG/MADGRAPH [22] for $W/Z+\gamma$). The total diboson background contribution is estimated to be $0.39 \pm 0.06(syst)$ for 35 pb^{-1} of integrated luminosity. The quoted systematic uncertainty includes uncertainties in the luminosity (11%), the SM diboson cross-sections (5%), the jet veto efficiency (6%), the acceptance due to PDFs (1%), the di-lepton trigger and identification efficiencies (4%) and pile-up effects (0.5%).

The hadronic dijets background contribution is negligible in the W^+W^- signal region as determined by PYTHIA MC and cross-checked by data.

9 Results

9.1 Summary of observations and predictions

The observed and expected number of events after applying all W^+W^- selection cuts are shown in Table 5. Both statistical and systematic uncertainties are given for all three di-lepton channels in the table. The overall signal to background ratio is about 4.3.

Final State	$e^+e^-E_{\rm T}^{\rm miss}$	$\mu^+\mu^-E_{\rm T}^{\rm miss}$	$e^\pm\mu^\mp E_{\rm T}^{\rm miss}$	combined
Observed Events	1	2	5	8
MC WW Signal	0.85±0.02±0.13	1.74±0.04±0.24	4.81±0.06±0.68	7.40±0.07±1.05
Backgrounds				
Top (MC)	0.04±0.02±0.03	0.15±0.06±0.08	0.36±0.10±0.19	0.55±0.12±0.30
W+jets (data)	0.08±0.05±0.03	0.00±0.29±0.10	0.46±0.12±0.17	0.54±0.32±0.21
DY (MC/data)	0.00±0.10±0.07	0.01±0.10±0.07	0.23±0.06±0.15	0.24±0.15±0.17
Other dibosons (MC)	0.05±0.01±0.01	0.10±0.01±0.01	0.24±0.05±0.03	0.39±0.04±0.06
Total Background	0.17±0.11±0.09	0.26±0.31±0.15	1.29±0.17±0.32	1.72±0.37±0.45
Signal / Background	5.0	6.7	3.7	4.3

Table 5: Summary of observed events and expected signal and background contributions in three di-lepton and combined channels. The first error is statistical, the second systematic. The methods used to determine the background contributions are indicated in the first column. Taking the systematic uncertainties from top and other dibosons as 100% correlated, but independent from the Drell-Yan (DY) and the W+jets systematic uncertainties (which are estimated from data), the combined systematic uncertainty for the total background is calculated to be $\sqrt{(0.30+0.06)^2+0.21^2+0.17^2}=0.45$. When the quoted errors are greater than the central values, the lower boundary of the background contribution should be taken as zero. The central value and statistical uncertainty for the Drell-Yan process estimation is MC based while the systematic uncertainties are derived from a data-driven method.

The kinematic distributions of the final W^+W^- candidates compared with the predicted W^+W^- signal and estimated background are shown in the following figures for leptons, di-leptons and di-lepton plus $E_{\rm T}^{\rm miss}$ systems. The leading and the sub-leading lepton $p_{\rm T}$ are shown in Fig. 5. The di-lepton system $p_{\rm T}$ and the ϕ angle difference between two leptons are shown in Fig. 6. Figure 7 shows the distributions of transverse mass $M_{\rm T}=\sqrt{(E_{\rm T}^{\ell 1}+E_{\rm T}^{\ell 2}+E_{\rm T}^{\rm miss})^2-(\vec{p}_{\rm T}^{\,\ell 1}+\vec{p}_{\rm T}^{\,\ell 2}+\vec{E}_{\rm T}^{\rm miss})^2}$ and transverse momentum $p_{\rm T}(\ell\ell E_{\rm T}^{\rm miss})$ of the di-lepton plus $E_{\rm T}^{\rm miss}$ system, where $E_{\rm T}^{\ell}$ and $\vec{p}_{\rm T}^{\,\ell}$ denote transverse energies and momenta for leptons, and $E_{\rm T}^{\rm miss}$ and $\vec{E}_{\rm T}^{\rm miss}$ denote missing transverse energy and momentum in the event. The MC results shown in these plots are normalized to the integrated luminosity of 35 pb^{-1} and the SM cross sections with event selection acceptance. These distributions are sensitive to new physics which could be revealed by anomalous triple gauge couplings.

9.2 W^+W^- detection sensitivity

We estimate the W^+W^- detection sensitivity using the log-likelihood ratio method as shown in Eqn. 2.

$$-2\ln Q=-2\ln\frac{L(\mathrm{s+b})}{L(\mathrm{b})};\quad L(\mathrm{s+b})=\frac{e^{-(N_\mathrm{s}+N_\mathrm{b})}(N_\mathrm{s}+N_\mathrm{b})^{N_\mathrm{obs}}}{N_\mathrm{obs}!},\quad L(\mathrm{b})=\frac{e^{-N_\mathrm{b}}(N_\mathrm{b})^{N_\mathrm{obs}}}{N_\mathrm{obs}!},\qquad(2)$$

where N_s, N_b and N_obs represent expected signal, background, and observed data events for the three di-lepton channels combined. To take into account the possibility of background fluctuations, 10 million pseudo-experiments were performed, using the expected number of background events as the mean value of a Poisson distribution to produce 'observed' events (N_obs) for each pseudo-experiment. The background uncertainty of 0.58 events is included as a Gaussian variation of the expected background yield. This uncertainty on the background estimate includes both statistical and systematic uncertainties.

With eight observed W^+W^- candidate events and 1.72± 0.58 (stat $\oplus$ syst) estimated background events, we estimate that the probability for the background to fluctuate up to at least the observed number

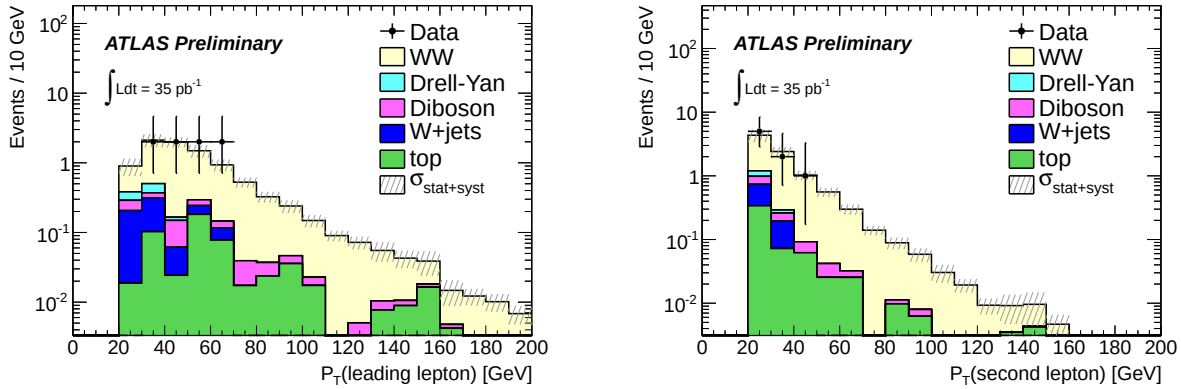

Figure 5: Distributions of leading (left) and sub-leading (right) lepton p_{T} for W^+W^- candidates. The points are the data and the stacked histograms are from MC predictions except the W+jets background, which is obtained from data-driven methods. The estimated uncertainties are shown as the hatched bands (stat $\oplus$ syst).

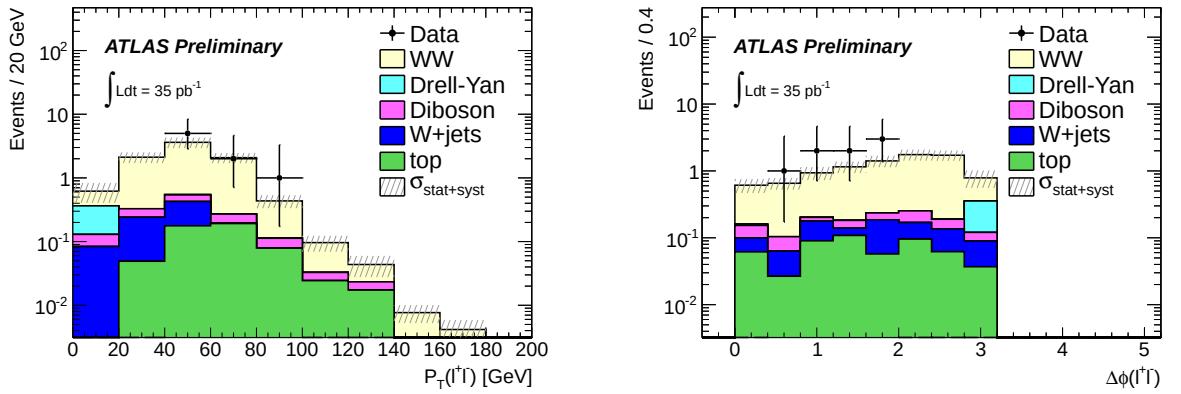

Figure 6: Distributions of di-lepton system p_{T} (left) and $\Delta\phi(\ell^+\ell^-)$ (right) for W^+W^- candidates. The points are the data and the stacked histograms are from MC predictions except the W+jets background, which is obtained from data-driven methods. The estimated uncertainties are shown as the hatched bands (stat $\oplus$ syst).

of events in the absence of the signal is 1.4×10^{-3}, corresponding to a significance of 3.0 standard deviations for the signal observation. The expected W^+W^- detection sensitivity from the MC simulation is 3.4 standard deviations, with a probability of 4.0×10^{-4} for the background-only hypothesis.

9.3 Measurement of the W^+W^- production cross section

The W^+W^- production cross section is determined in three di-lepton channels using a maximum log-likelihood fitting method. The log-likelihood function based on the Poisson statistics is constructed using the selected MC and data events as shown in Eqn. 3:

$$F = \ln \prod_{i=1}^{3} \frac{e^{-(N_{\mathrm{s}}^i + N_{\mathrm{b}}^i)} (N_{\mathrm{s}}^i + N_{\mathrm{b}}^i)^{N_{\mathrm{obs}}^i}}{N_{\mathrm{obs}}^i!}, \quad N_{\mathrm{s}}^i = \sigma_{WW} \times Br^i \times \mathscr{L} \times A^i, \tag{3}$$

where $i = 1,2,3$ runs over three channels. N_{s}^i represents the fitted signal events containing the information of the measured WW cross-section, N_{b}^i and N_{obs}^i represent the expected number of background events and

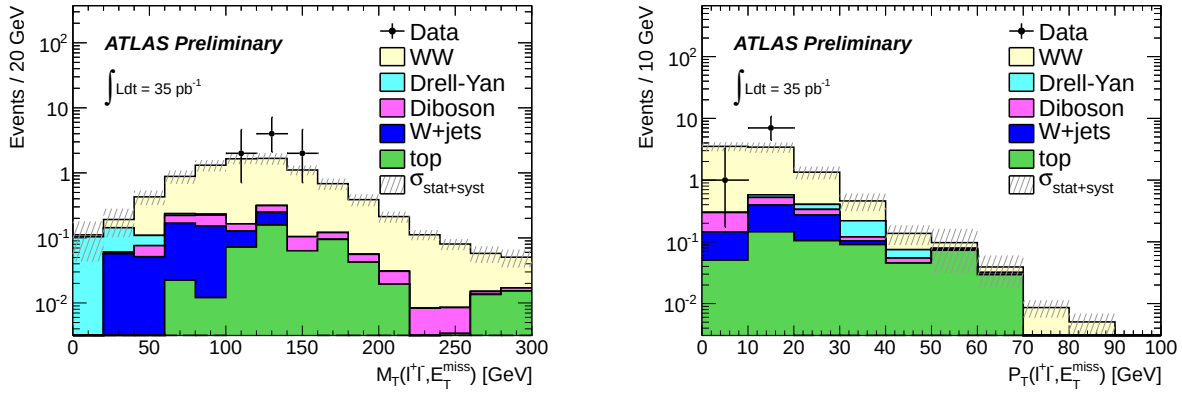

Figure 7: Distributions of M_{T} (left) and p_{T} (right) of the di-lepton+$E_{\mathrm{T}}^{\mathrm{miss}}$ system for the W^+W^- candidates. The points are the data and the stacked histograms are from MC predictions except the W+jets background, which is obtained from data-driven methods. The estimated uncertainties are shown as the hatched bands (stat $\oplus$ syst).

observed events for the i-th di-lepton channel, respectively. Br^i is the leptonic branching ratio, $\mathscr{L}$ is the integrated luminosity, and A^i is the signal acceptance corrected by the selection efficiency difference between data and MC. The W^+W^- cross section (σ_{WW}) is determined by maximizing the log-likelihood function F. The fitted W^+W^- cross sections for three channels individually and combined are listed in Table 6.

Channels	N_{s}(SM)	N_{b}	N_{obs}	σ_{WW} [pb]
$e^+e^-E_{\mathrm{T}}^{\mathrm{miss}}$	0.85	0.17	1	45^{+74}_{-38}
$\mu^+\mu^-E_{\mathrm{T}}^{\mathrm{miss}}$	1.74	0.26	2	46^{+47}_{-29}
$e^\pm\mu^\mp E_{\mathrm{T}}^{\mathrm{miss}}$	4.81	1.29	5	36^{+25}_{-19}
Total	7.40	1.72	8	40^{+20}_{-16}

Table 6: Inputs for the WW cross-section measurements and the corresponding extracted results. N_{s}(SM), N_{b}, and N_{obs} denote number of the SM expected signal, estimated background, and observed events, respectively. σ_{WW} is the cross section from the maximum log-likelihood fitting. Only statistical uncertainties are given.

The combined W^+W^- cross section together with statistical and systematic uncertainties is

$$\sigma_{WW} = 40^{+20}_{-16}(\mathrm{stat}) \pm 7(\mathrm{syst})\ \mathrm{pb}.$$

The statistical uncertainty (44%) is the dominant uncertainty for this measurement. The total systematic uncertainty (16.4%) includes the luminosity uncertainty ($\Delta\mathscr{L}/\mathscr{L} = 11\%$), acceptance uncertainty ($\Delta A/A = 7.4\%$), and background estimation uncertainty ($\Delta N_{\mathrm{b}}/N_{\mathrm{b}} = 34\%$). The relative systematic uncertainty for the cross section measurement is estimated as

$$\sigma_{\mathrm{syst}}/\sigma_{WW} = \sqrt{(\Delta\mathscr{L}/\mathscr{L})^2 + (\Delta A/A)^2 + (\Delta N_{\mathrm{b}}/(N_{\mathrm{obs}} - N_{\mathrm{b}}))^2},$$

which is derived from the formula $\sigma_{WW} = \frac{N_{\mathrm{obs}} - N_{\mathrm{b}}}{A\,\mathscr{L}\,Br}$.

10 Summary

The W^+W^- production cross section in pp collisions at $\sqrt{s} = 7$ TeV is measured using 35 pb^{-1} of data collected by the ATLAS detector during 2010. The measurement is conducted using three W^+W^- leptonic decay channels. A total of eight candidates are selected with an estimated background of 1.7 $\pm$ 0.6 events. The probability for the estimated background to fluctuate up to at least the observed eight events is 1.4×10^{-3}, corresponding to a signal significance of 3.0 standard deviations. The measured cross section is 40^{+20}_{-16}(stat)$\pm$7(syst) pb, consistent with the SM NLO prediction of 46 ± 3 pb.

References

[1] J. Ohnemus, *An order-α_s calculation of hadronic W^-W^+ production*, Phys. Rev. **D44** (1991) 1403–1414.

[2] S. Frixione, *A next-to-leading order calculation of the cross-section for the production of W^+W^- pairs in hadronic collisions*, Nucl. Phys. **B410** (1993) 280–324.

[3] J. Ohnemus, *Hadronic ZZ, W^-W^+, and $W^\pm Z$ production with QCD corrections and leptonic decays*, Phys. Rev. **D50** (1994) 1931–1945, arXiv:hep-ph/9403331.

[4] L. J. Dixon, Z. Kunszt, and A. Signer, *Helicity amplitudes for O(alpha-s) production of W^+W^-, $W^\pm Z$, ZZ, $W^\pm\gamma$, or $Z\gamma$ pairs at hadron colliders*, Nucl. Phys. **B531** (1998) 3–23, arXiv:hep-ph/9803250.

[5] L. J. Dixon, Z. Kunszt, and A. Signer, *Vector boson pair production in hadronic collisions at order α_s : Lepton correlations and anomalous couplings*, Phys. Rev. **D60** (1999) 114037, arXiv:hep-ph/9907305.

[6] J. M. Campbell and R. K. Ellis, *An update on vector boson pair production at hadron colliders*, Phys. Rev. **D60** (1999) 113006, arXiv:hep-ph/9905386.

[7] ATLAS Collaboration, G. Aad et al., *The ATLAS experiment at the CERN Large Hadron Collider*, JINST **3** (2008) S08003.

[8] ATLAS Collaboration, G. Aad et al., *Luminosity Determination in pp Collisions at sqrt(s)=7 TeV Using the ATLAS Detector at the LHC*, arXiv:1101.2185 [hep-ex].

[9] S. Frixione and B. R. Webber, *Matching NLO QCD computations and parton shower simulations*, JHEP **06** (2002) 029, hep-ph/0204244.

[10] P. M. Nadolsky et al., *Implications of CTEQ global analysis for collider observables*, Phys. Rev. **D78** (2008) 013004, arXiv:0802.0007 [hep-ph].

[11] G. Corcella et al., *HERWIG 6.5: an event generator for hadron emission reactions with interfering gluons (including supersymmetric processes)*, JHEP **0101** (2001) 010, arXiv:hep-ph/0011363.

[12] J. M. Butterworth et al., *Multiparton interactions in photoproduction at HERA*, Z. Phys. **C72** (1996) 637–646.

[13] T. Binoth, M. Ciccolini, N. Kauer, and M. Kramer, *Gluon-induced W-boson pair production at the LHC*, JHEP **12** (2006) 046, arXiv:hep-ph/0611170.

[14] ATLAS Collaboration, G. Aad et al., *The ATLAS Simulation Infrastructure*, Eur.Phys.J. **C70** (2010) 823–874, arXiv:1005.4568 [physics.ins-det].

[15] S. Agostinelli et al., *GEANT4: A Simulation toolkit*, Nucl.Instrum.Meth. **A506** (2003) 250–303.

[16] ATLAS Collaboration, G. Aad et al., *Measurement of the $W \to l\nu$ and $Z/\gamma^* \to ll$ production cross sections in proton-proton collisions at $\sqrt{s}$ = 7 TeV with the ATLAS detector*, JHEP **12** (2010) 060, arXiv:1010.2130 [hep-ex].

[17] M. Cacciari, G. P. Salam, and G. Soyez, *The anti-k_t jet clustering algorithm*, JHEP **04** (2008) 063, arXiv:0802.1189 [hep-ph].

[18] M. Cacciari and G. P. Salam, *Dispelling the N^3 myth for the k_t jet-finder*, Phys. Lett. **B641** (2006) 57–61, arXiv:hep-ph/0512210.

[19] M. Cacciari, G. P. Salam, G. Soyez, http://fastjet.fr/.

[20] ATLAS Collaboration, *Jet energy scale and its systematic uncertainty in ATLAS for jets produced in proton-proton collisions at $\sqrt{s} = 7$ TeV*, ATLAS-CONF-2010-056, 2010.

[21] J. M. Campbell et al., *Normalizing weak boson pair production at the large hadron collider*, Phys. Rev. **D80** (2009) 054023, arXiv:0906.2500 [hep-ph].

[22] J. Alwall et al., *MadGraph/MadEvent v4: The new web generation*, JHEP **09** (2007) 028, arXiv:0706.2334 [hep-ph].

A Candidate event displays

This appendix gives event displays and basic kinematic information for three W^+W^- candidate events, one from each dilepton channel.

A.1 eμ channel

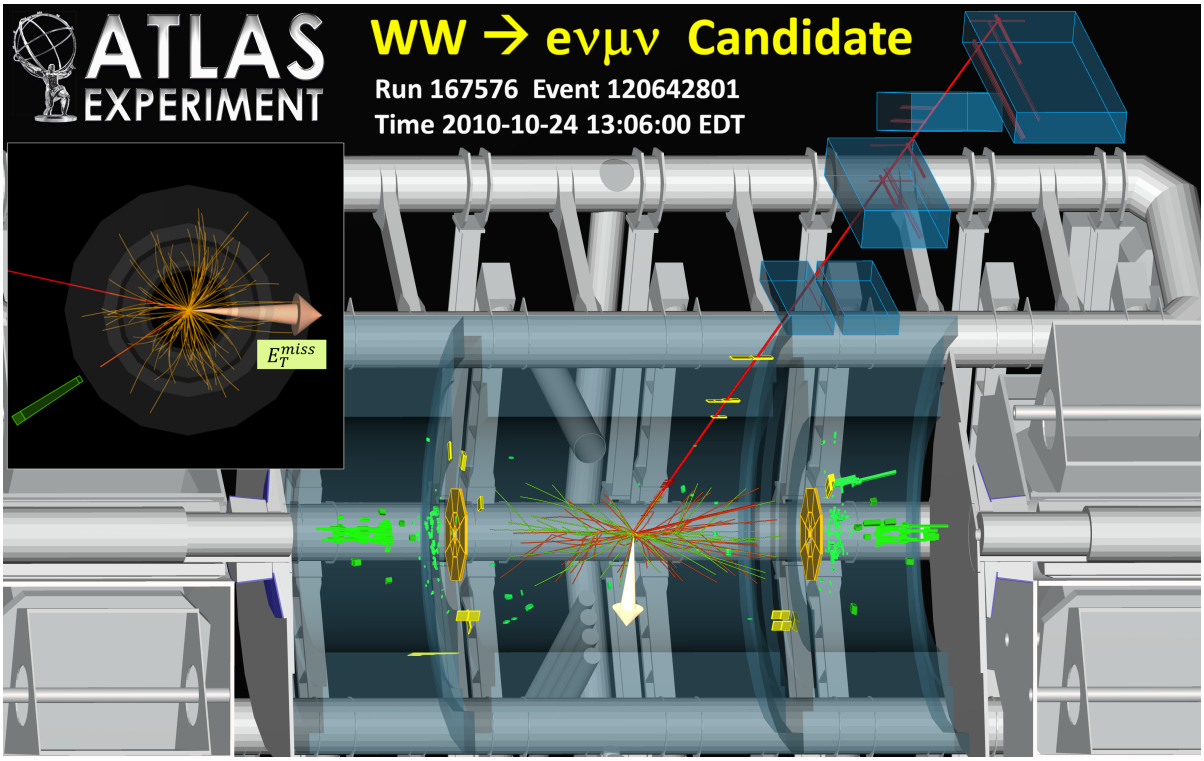

Figure 8: Event display of a $WW \to e\mu\nu\nu$ candidate event.

Run number	Event number	$p_T^{\mu^-}$ [GeV]	η^{μ^-}	ϕ^{μ^-}	$p_T^{e^+}$ [GeV]	η^{e^+}	ϕ^{e^+}	$E_{\mathrm{T}}^{\mathrm{miss}}$ [GeV]	$\phi_{E_{\mathrm{T}}^{\mathrm{miss}}}$
167576	120642801	67.8	-0.63	0.20	21.2	-1.56	-0.56	68.8	-3.08

Table 7: Run and event number and basic kinematic information of the event shown in Fig. 8.

A.2 ee channel

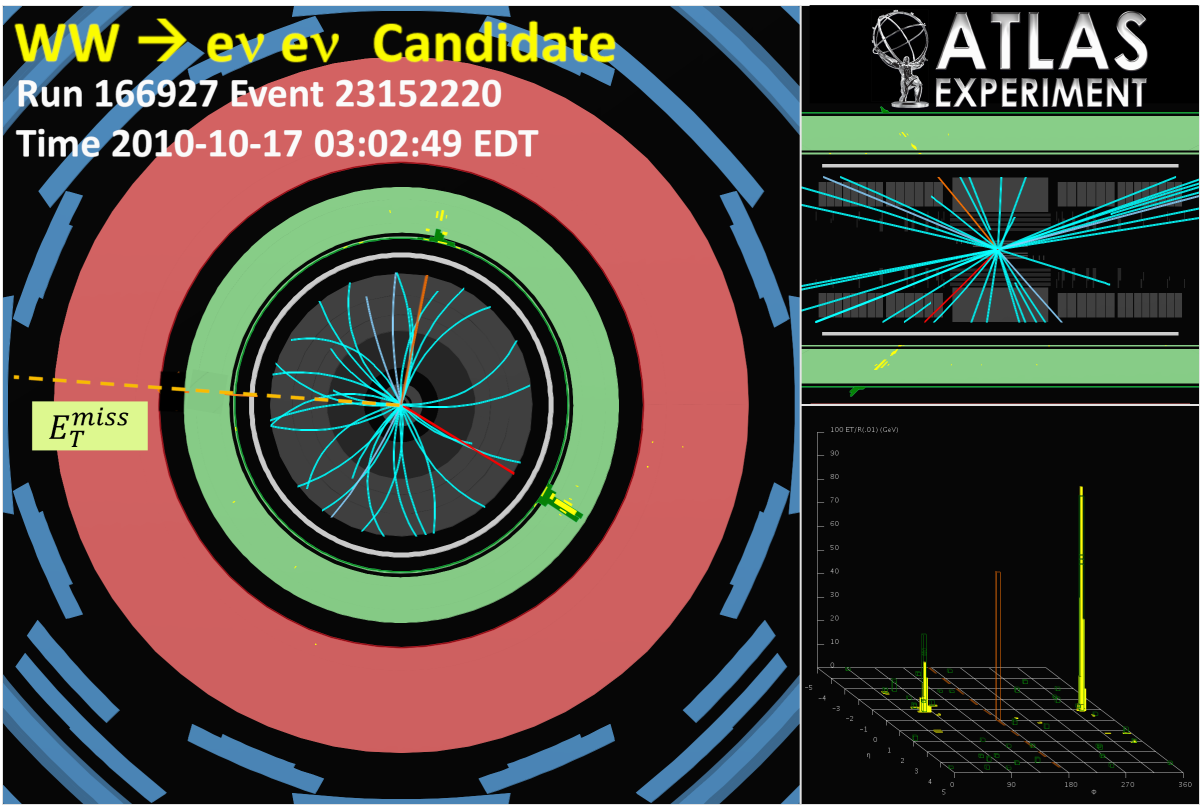

Figure 9: Event display of a $WW \to ee\nu\nu$ candidate event.

Run number	Event number	$p_T^{e^-}$ [GeV]	η^{e^-}	ϕ^{e^-}	$p_T^{e^+}$ [GeV]	η^{e^+}	ϕ^{e^+}	$E_{\mathrm{T}}^{\mathrm{miss}}$ [GeV]	$\phi_{E_{\mathrm{T}}^{\mathrm{miss}}}$
166927	23152220	25.3	-0.75	1.36	65.1	-0.89	-0.55	69.9	3.04

Table 8: Run and event number and basic kinematic information of the event shown in Fig. 9.

A.3 $\mu\mu$ channel

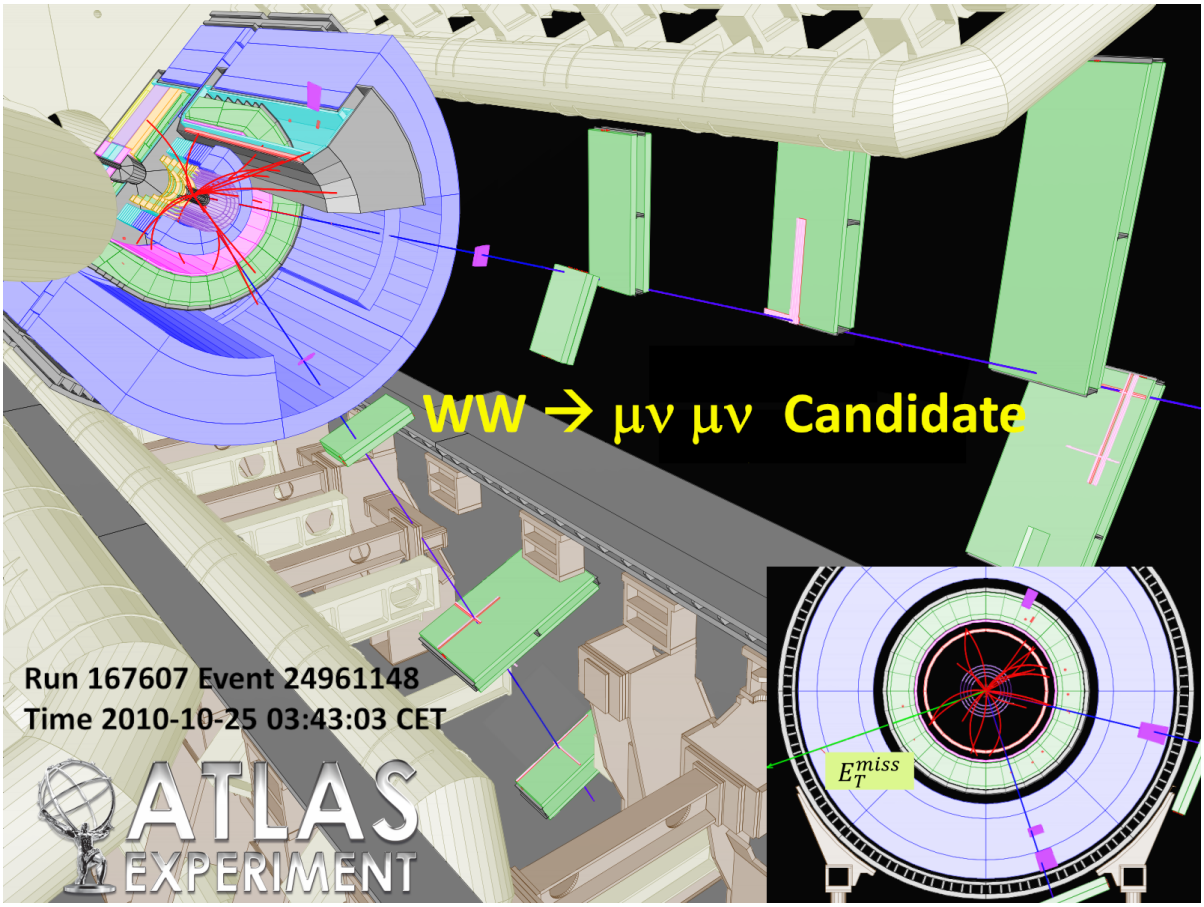

Figure 10: Event display of a $WW \rightarrow \mu\mu\nu\nu$ candidate event.

Run number	Event number	$p_T^{\mu^-}$ [GeV]	η^{μ^-}	ϕ^{μ^-}	$p_T^{\mu^+}$ [GeV]	η^{μ^+}	ϕ^{μ^+}	$E_{\mathrm{T}}^{\mathrm{miss}}$ [GeV]	$\phi_{E_{\mathrm{T}}^{\mathrm{miss}}}$
167607	24961148	25.3	-0.60	-1.86	40.5	-1.01	-2.92	61.1	0.33

Table 9: Run and event number and basic kinematic information of the event shown in Fig. 10.